J. Phys. D: Appl. Phys. **26** (1993) 2266–2271. Printed in the UK

Electron backscattering and secondary electron emission from carbon targets: comparison of experimental results with Monte Carlo simulations

H Farhang†, E Napchan‡ and B H Blott†

† Physics Department, University of Southampton, Southampton SO9 5NH, UK
‡ Department of Materials, Imperial College, London SW7 2BP, UK

Received 25 February 1993, in final form 16 August 1993

Abstract. Electron backscattering (EBS) and secondary electron emission (SEE) yield have been measured for bulk carbon with a density of 1.8 g cm^{-3}, for primary electron energies in the range from 100 to 500 eV and from 12 to 1000 eV respectively. The backscattering results were in agreement with an empirical formula to within 2%. The SEE yield value was 0.04 at lowest measured energy (12 eV) and reached a maximum value of 0.54 at about 300 eV. The backscattering coefficients and SEE yield have also been calculated using a Monte Carlo simulation for the energy range from 12 to 1000 eV. In the simulation, two different energy loss characteristics were used. The first was obtained from a set of optical data and gave good agreement with the experimental SEE yield but poor agreement with the backscattering data. The second was obtained from a modified Bethe energy loss function which fitted the backscattering data well. Using the Bethe loss function for each primary electron, the SEE yield was calculated for every path length between scattering events by dividing the primary electron energy lost per unit path length by the *average* energy required to create a secondary electron. The SEE data was fitted on the assumption that the *average* energy to create a secondary varied with primary electron energy according to a four parameter function. Comparison of the calculated SEE yield with the experimental SEE yield, as a function of incident angle of the primary beam, was good over the energy range from 100 to 500 eV.

1. Introduction

When a beam of electrons falls onto a surface of a solid secondary electrons are released. These secondary electrons can play an important role in determining the sheath potential at a surface exposed to plasma [1–3] which in turn accelerates ions and retards electrons. This affects the sputtering rate of atoms from the walls and hence the impurity flux to the plasma. Surfaces also become altered by erosion, ion implantation and deposition while exposed to plasma. Such processes are particularly troublesome in plasma devices designed to extract power from nuclear fusion. These devices employ plasma limiters at the walls to control the impurity flux, and one of the materials used for this purpose is graphite.

There have been a number of reports of SEE yield data for different types of graphite [2, 4–6]. We have reported in earlier papers [2, 4] the changes in secondary electron emission (SEE) yield from graphite due to hydrogen ion implantation. In this paper we report the comparison between new backscattering (BS) experimental data and SEE yield data, for pocographite, with a new Monte Carlo simulation of backscattering over the energy range from 12 to 1000 eV. We also compare the experimental SEE yields, as a function of the beam incidence angle [4], with our experimental simulation. The analysis technique was originally developed for use in scanning electron microscopy where the BS coefficient η is used to provide a measure of atomic number contrast from a specimen, and also for measuring the thickness of metal plating [7].

2. Experimental method

The experimental system used to measure electron backscattering from carbon samples (pocographite) was a standard LEED–Auger four-grid system, similar to that described by Woods *et al* [2, 5]. Measurement of both the BS coefficient and the SEE yield were carried out in an ultrahigh vacuum (UHV) system with a base pressure

0022-3727/93/122266+06$07.50

of 10^{-9} Torr. The system was initially pumped down using a rotary pump, followed by oil diffusion pumping. To prevent any oil vapour from getting into the vacuum system from the rotary pump, a molecular sieve trap was used and the low vapour pressure from the diffusion pump oil (Santovac 5) was trapped by liquid nitrogen cooling. The system was then baked for 48 h at 200 °C. The samples of pocographite were treated to remove any grease or oil contamination immediately before their installation in the vacuum system: the samples were ultrasonically cleaned in trichloroethane for 30 min and then in deionized water for a further 30 min. After installation in UHV the samples were heated to 600 °C by electron beam bombardment from the back for 30 min.

During the experimental measurements the energy of the primary electron beam was varied by applying a negative bias, of between −100 V and −500 V, to the electron gun cathode. This was controlled by a microcomputer through a 12-bit DAC unit and a high-voltage amplifier; the data were recorded by the computer through a 12-bit ADC and signal conditioning amplifiers. The experimental measurements were made in the following way. The carbon target, in the shape of a square of area 1 cm^2, and the LEED–Auger collector were held at earth potential, and a negative bias of −50 V was applied to grids 2, 3, and 4 of the LEED–Auger system. The current to the target I_T, and the current to the collector I_c were sampled with the multiplexed ADC and the backscattering coefficient was obtained from:

$$\eta = \frac{I_c}{(I_c + I_T)}. \tag{1}$$

For each experimental data point eight independent measurements were taken. The duration time for each data point was set at one second, the settling time of the ammeter.

For SEE measurements at low primary energies a cylindrical triode arrangement was used as illustrated in cross section in figure 1. A new sample of pocographite in the shape of a cylinder with internal and external diameters of 2 and 3 cm respectively and a height of 3 cm was treated as above. The primary electrons were produced from an axially located hot filament and were accelerated towards the target by biasing the filament negatively with respect to a concentric grid and the target. The secondary electrons produced by the target were then collected by the grid, positively biased with respect to the target. The current to the sample and grid were measured simultaneously by a Keithley multimeter Model 177 and an opto-isolated ammeter respectively. The latter was built for the purpose of measuring grid current while biasing the grid by a positive voltage. The SEE yield was then calculated as a function of the primary energy following Bruining [8]. The measured currents to the target I_T and the grid I_G, and the secondary electron current I_S are given by the following three equations:

$$I_G = f I_p + I_S \tag{2}$$

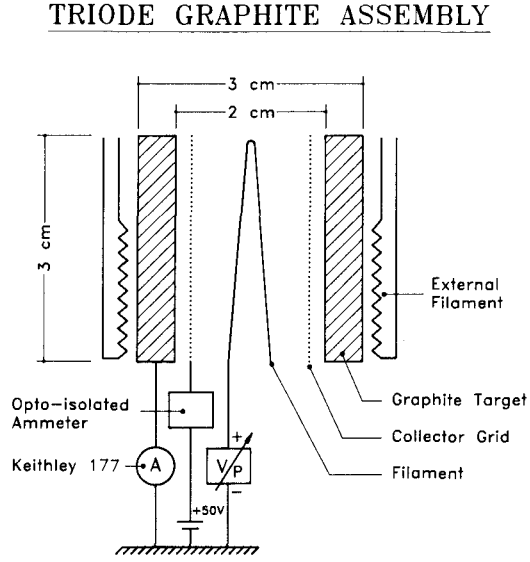

Figure 1. Schematic cross section of cylindrical triode used for measuring SEE yield δ.

$$I_S = \delta(1 - f)I_p \tag{3}$$

$$I_T = (1 - f)I_p - I_S \tag{4}$$

where I_p is the primary electron current incident on the target, and f is the fraction of the primary current intercepted by the grid which is assumed to be the fraction of the anode surface occluded by the grid. Combining these gives the secondary yield δ in terms of the measured target and grid currents:

$$\delta = 1 - \frac{I_T}{(1 - f)(I_T + I_G)}. \tag{5}$$

At high electron beam energies (about 1 keV) some of the high-energy backscattered electrons could pass through the grid and hit the target a second time. The flux of such electrons is likely to depend on the grid bias and therefore we carried out preliminary experiments in which the bias was first set at values between 10 and 50 V and then set at 1/4, 1/3 and 1/2 of the primary electron energy. The SEE yield as a function of primary energy remained unchanged, within experimental uncertainty, for biases exceeding 30 V. Each data point with its standard deviation (about ±0.01) is the result of averaging eight independent measurements. The SEE yield was measured over the extended primary energy range of 1000 eV down to 12 eV, about 40 eV lower than our earlier reported results [2, 4]. Below 12 eV the experimental uncertainty (indicated by the standard deviation on the data of 0.1) was much greater than the value at higher primary energies (0.01).

3. Calculation of the backscattering and SEE coefficients

For backscattering two methods will be considered: empirical formulae, usually based on curve fitting to experimental data, and Monte Carlo simulations in

which the backscattering is one amongst many of the parameters that can be calculated. For the SEE yield, experimental data are compared with Monte Carlo simulations combined with empirical formulae.

3.1. Empirical calculations for evaluation of η

Everhart [9] obtained relations for the backscattering coefficient η as a function of film thickness and beam energy and used these to derive an empirical expression for the bulk backscattering coefficient:

$$\eta = \frac{[\alpha - 1 + (0.5)^{\alpha}]}{(\alpha + 1)} \tag{6}$$

where $\alpha = 0.045Z$ was used by Everhart to fit the above expression to his experimental data and Z is the atomic number of the specimen material.

According to Sogard [7] values calculated from equation (6) are 'known' to be too high for high-Z materials. Verma [10] has suggested that the parameter α should also depend on the incident electron energy, which for the case of carbon is of the form:

$$\alpha = 5.49E^{-0.36} \tag{7}$$

where E is the electron energy in eV.

3.2. Monte Carlo (MC) simulation of electron/matter interactions

The Monte Carlo simulation is based on the complete evaluation of a large number of single interactions, each of which uses some random data as part of the calculation. Although the evaluation of parameters for a single particle cannot represent the actual process, a large number of such particles will be quantitatively and qualitatively representative.

The interactions between an electron and a solid can be separated into elastic and inelastic types. The former results in large scattering angles without changes in the electron energy, while the latter processes allow a decrease in the electron energy with relatively small angles of scatter. These interactions appear in the calculation as the energy loss per unit path length, covering all the inelastic interactions, and the scattering parameters which affect the scattering angles and the path length between scattering events. The simulation assigns both an energy loss and a change in direction after each interaction event. The method is based on the work of Myklebust *et al* [11], on the various publications by Joy (e.g. [12]), on the work by Liljequist [13], and on data from optical experiments [14].

We have used the MC method to follow individual primary electrons until they escape the material through the surface by which they entered (i.e. backscattered electrons) or until they have insufficient energy to escape. The MC simulation program records for each backscattered electron its energy and exit direction allowing, if needed, further analysis.

The number of secondary electrons generated per unit length along the whole primary electron trajectory in the material is assumed to be proportional to the energy loss per unit length $\mathrm{d}E/\mathrm{d}S$, and is given by:

$$N = \frac{(\mathrm{d}E/\mathrm{d}S)}{U} \tag{8}$$

where U is the average energy required to generate a secondary electron, which may be a function of primary beam energy [15]. The probability of escape from the surface of the excited secondary electrons is represented by an exponential function of the depth of generation x:

$$p(x) = 0.5\exp(-x/l) \tag{9}$$

where l is called the escape depth. The transport to, and escape from, the surface of the secondaries was not modelled by the MC method. For higher energy primary electrons, in the keV range well above the energies of interest here, secondary processes have been modelled by the MC method by Valkealahti *et al* [16].

The primary electron energy loss per unit trajectory length travelled in the material is evaluated in the current simulation using two methods: either using the optical data model of Ashley [14], or using a modified form [17] of the Bethe stopping power relation:

$$\frac{\mathrm{d}E}{\mathrm{d}S} = -78\,500\frac{\rho Z}{AE}\log\left(\frac{1.166E}{J_{\mathrm{p}}}\right) \text{ keV cm}^{-1} \tag{10}$$

where ρ is the material density in g cm^{-3}, Z the atomic number, A the atomic mass in g mole^{-1}, E is the instantaneous electron energy in keV, and J_{p} is given by:

$$J_{\mathrm{p}} = \frac{J}{1 + k(J/E)} \tag{11}$$

where $k = 0.822$ and J is the mean ionization potential of the specimen material in keV.

The advantage of using such a relation is that it keeps the original form of the Bethe stopping power relation for high energies, whilst also being valid for the low electron energy range. Joy and Luo [17] suggest that the validity of this stopping power relation extends down to a few electron volts, which agrees well with the statistical model and the experimental data reported by Tung *et al* [18].

The electron scattering parameters (scattering angle and mean free path) are calculated using a relativistic screened Rutherford cross section with a correction factor due to Liljequist [13] based on cross section calculations computed from partial wave analysis.

Using linear interpolation and extrapolation of tabulated electron energies [13], a correction factor κ was found and used to calculate the mean free path λ between scattering events:

$$\lambda = \frac{\kappa A}{\rho\sigma N} \tag{12}$$

where λ is in cm, A is the atomic weight in g mole^{-1}, N is Avogadro's number, ρ is the layer density in g cm^{-3}, σ is the Rutherford cross section in cm^2. The step length s between scattering events is then calculated from:

$$s = -\lambda \log_e(R) \tag{13}$$

where R is a random number between 0 and 1. The scattering angles are calculated using the equations given by Neubury and Myklebust [19].

The property required to calculate the energy loss dE/dS and the mean free path λ in the optical model is the complex dielectric function [14]. This was calculated from the experimentally obtained complex refractive index [20], and dE/dS and λ were numerically evaluated using equations (10) and (12) [14].

Using the optical data [20], the stopping power dE/dS at energy E is calculated following Ashley [14]:

$$\frac{dE}{dS} = \frac{1}{\pi E}\int_0^{E/2} d\omega\, \omega\, \mathrm{Im}[-1/\varepsilon(\omega)]G(\omega/E) \tag{14}$$

with

$$G(a) = \ln\frac{1}{4a} - \frac{3}{4}a - \frac{a}{4}\ln\frac{4}{a} + \frac{1}{2}a^{3/2} - \frac{a^2}{16}\ln\frac{4}{a} - \frac{31}{48}a^2 \tag{15}$$

where $a = \omega/E$ and $\varepsilon(\omega)$ is the complex dielectric constant of the medium at zero wavevector and frequency ω. The optical data were measured over the range 0.5 to 62 eV for arc evaporated carbon films of density 1.90 ± 0.05 g cm^{-3} [20]. The mean free path is then calculated, again following Ashley [14]:

$$\frac{1}{\lambda} = \frac{1}{2\pi E}\int_0^{E/2} d\omega\ \mathrm{Im}\left[-\frac{1}{\varepsilon(\omega)}\right]L(\omega/E) \tag{16}$$

where

$$L(a) = (1-a)\ln\left(\frac{4}{a}\right) - \frac{7}{4}a + a^{3/2} - \frac{33}{32}a^2. \tag{17}$$

The Monte Carlo simulations were performed on a 486 microcomputer using the package MC-SET† originally designed for use with scanning electron microscopes. The calculation proceeded in two stages, firstly the backscattering was calculated from the energy loss and electron scattering relations, then the secondary emission results were fitted by adjusting the generation energy U, for the number of secondaries excited (equation (8)).

4. Results

Figure 2 compares various models for the backscattering coefficient with the experimental data. The data were recorded for electron beam energies from 100 to 500 eV under normal beam incidence on a bulk carbon target. The empirical model due to Verma [10] and two variants

† MC-SET available from Dr Eli Napchan, Department of Materials, Imperial College, London SW7 2BP, UK.

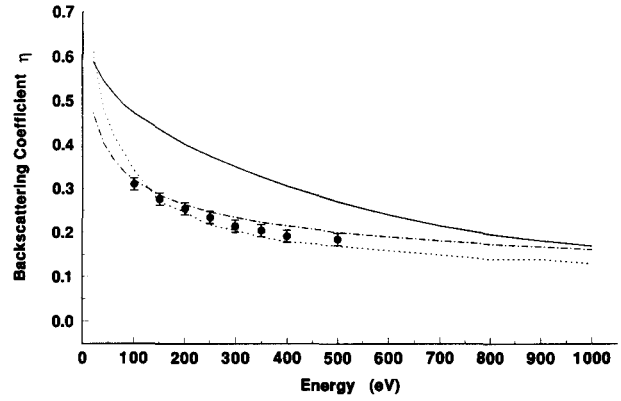

Figure 2. Experimental data (points with error bars) compared with simulations for the backscattering coefficient η as a function of incident electron energy. The optical data model (full curve) and the Liljequist corrected model (dotted curve) are two versions of the MC calculation. The predictions from the Verma empirical model are also shown (chain curve).

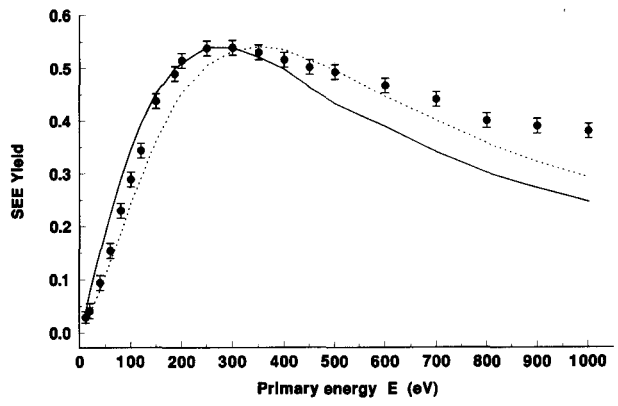

Figure 3. The comparison of the experimental SEE yield δ (points with error bars), as a funciton of incident electron energy, with two simulation models. The optical data model (full curve) and the Liljequist corrected model (broken curve) are two versions of the MC calculation.

of the Monte Carlo simulation are shown: one uses the electron mean free path given by the modified Rutherford cross section proposed by Liljequist [13], and the other uses optical data [14] for calculating mean free path and energy loss. The Verma empirical formula and the Liljequist corrected MC simulation show excellent agreement with the experimental data. However the MC simulation based on the optical model predicts some 50% greater backscattering. In the case of the SEE yield shown in figure 3 the values for U were chosen so that the maxima for the two models matched the experimental value: for the optical model $U = 101$ eV and for the Liljequist model $U = 125$ eV. The two variants of the MC simulations for the SEE yield were compared with experimental data over the energy range 12 to 1000 eV. The escape depth of the secondaries was chosen to be 18 Å in agreement with Ohya *et al* [21], and also with Voreades' estimate of 20 Å [22] from experimental data. As can be seen neither of the models appears to account for the observations if the 'scaling factor' U is maintained constant. However, it has been suggested by Ohya *et al* [15] that U increases with energy. We discuss this in the following section.

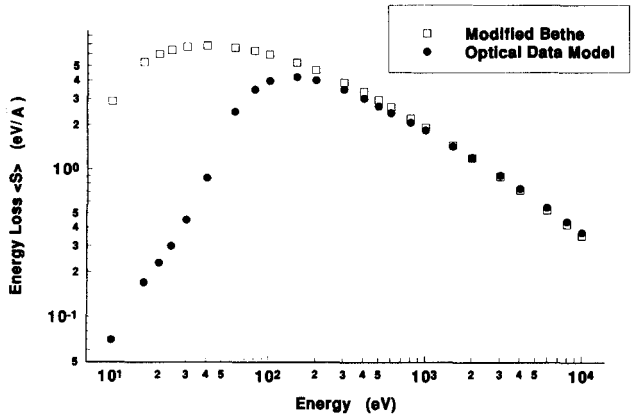

Figure 4. Electron energy loss as a function of electron energy in graphite according to the modified Bethe equation and an optical data model [14, 20].

Finally, we have compared the calculated simulation with the data on angular dependence of secondary emission reported by Pedgley *et al* [14]. Figure 7 (see later) shows the data, scaled to the secondary emission at normal incidence, compared with the Liljequist model: they agree within the experimental uncertainty.

5. Discussion

Two parameters in the MC simulation algorithm can be adjusted to account for the discrepancy between the experimental backscattering data and the model simulation. The first is the electron mean free path and the second is the energy loss per unit path length. Changing the electron mean free path of the optical model does not produce any significant change in the backscattering coefficient η. However, increasing the energy loss values (from the optical model values, as given in figure 4, towards values given by the modified Bethe equation) results in backscattering close to that obtained experimentally as well as to the prediction of the Verma empirical model. The MC simulation (with the Liljequist correction to the mean free path and the modified Bethe equation for the energy loss) agrees better with experiment than the optical model, possibly down to electron energies as low as 12 eV, although there still remains a problem with the secondary yield.

Ohya *et al* [15] have addressed the modelling of secondary electron emission by varying, wth primary energy, the average energy required to generate a secondary electron. Over the primary energy range 50 to 500 eV they determined that U increased from 78 to 171 eV. There is some justification for this in that the measured secondary electron energy spectrum does vary with primary electron energy. Furthermore, as the primary electron energy is increased, electrons from deeper energy levels are excited and emitted. For our experimental data we have chosen to fit a four parameter function for the *average* energy to excite a secondary electron U:

$$U = U_0 + \beta E + \gamma[1 - \exp(-E/E_0)] \qquad (18)$$

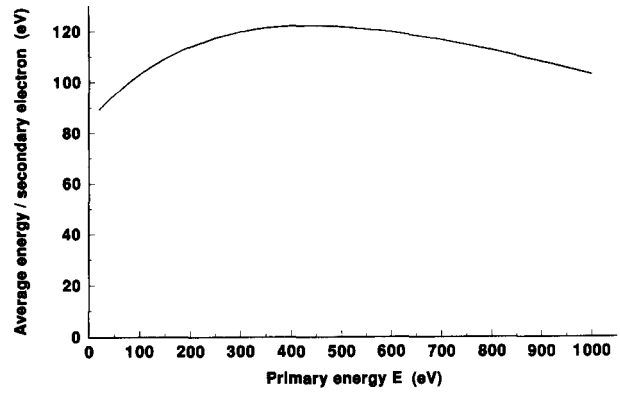

Figure 5. The average energy for generating a secondary electron as a function of primary energy. The parameters for the best fit were: $U_0 = 85$ eV, $\beta = -0.06$, $\gamma = 80$ eV, $E_0 = 280$ eV.

where U_0 and γ define initial and asymptotic values for U respectively, E_0 defines a characteristic scale energy and the linear coefficient β accounts for the misfit in the gradient at high primary energy. The last is least justifiable in terms of the secondary electron energy distribution which remains relatively invariant as the primary energy increases above several hundred electron volts. Figure 5 shows the values of U used, and figure 6 shows the experimental results compared with the simulation (using the Liljequist correction and the modified Bethe stopping power relation). A chi square test for the goodness of fit showed a discrepancy of one standard deviation. These results seem to suggest that different mechanisms may operate in the low- and the high-energy ranges, a change over occurring in the mid range of energy. It may be fortuitous but it is interesting to note that the maximum of U in figure 5 occurs at a primary energy at which the mean free path for primaries λ equals the secondary escape depth l. A likely mechanism to make up the deficit of secondaries in the model is the cascade process [23] that takes place as the secondaries propagate to the surface, which is not specifically modelled in this MC calculation. There is also some slight evidence from the backscattering results (see figure 2) that above 500 eV the Liljequist model does not provide enough backscattered electrons. In addition to including a model for the secondary electron cascade process perhaps some estimate needs to be included for the contribution to electron backscattering from coherent scattering by the crystalline lattice.

6. Conclusion

We have discussed MC models for calculating the electron backscattering coefficient and the secondary electron yield as a function of incident electron energies in the range from 12 to 1000 eV. We conclude that the model based on the Liljequist correction to the energy loss per unit length satisfactorily accounts for the backscattering data. This model also described the SEE yield if the average energy to generate a secondary electron U is adjusted empirically using a four parameter

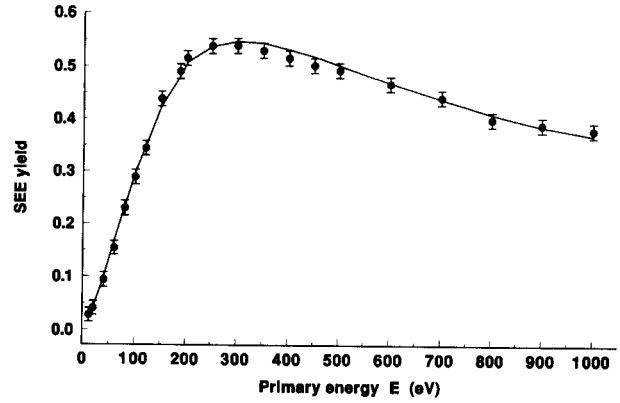

Figure 6. Comparison of the experimental data for the SEE yield δ with a fitted simulation. The points with error bars represent the experimental data. The full curve shows the simulation result based on the fitted function of figure 5 for U.

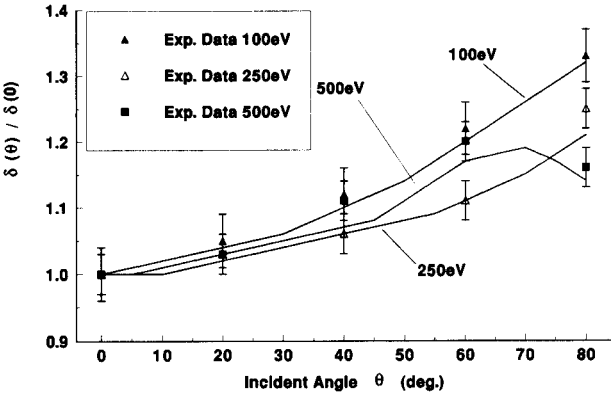

Figure 7. Experimental and theoretical SEE yield δ as a function of the macroscopic angle of incidence of the primary electrons for three different primary electron energies. The data are from a solid carbon target with an optically rough surface [4].

fit. The model also accounted well for the angular dependence of the secondary electron emission yield over the energy range from 100 to 500 eV.

Acknowledgments

The authors wish to record their appreciation for the interest and critical guidance accorded them by Dr G M McCracken. They also wish to acknowledge the financial support provided by AEA Fusion, Culham Laboratory, for the experimental phase of this work.

References

[1] Stangeby P C 1986 *Physics of Plasma Wall Interactions in Controlled Fusion, NATO ASI Series B* vol 131 ed D E Post and R Behrisch (New York: Plenum) pp 41–97
[2] Woods M E, Hopkins B J, Matthews G F, McCracken G M, Sewell P M and Farhang H 1987 *J. Phys. D: Appl. Phys.* **20** 1136–42
[3] Matthews G F, McCracken G M, Sewell P M, Woods M E and Hopkins B J 1987 *J. Nucl. Mater.* **145–7** 225–30
[4] Pedgley J M, McCracken G M, Farhang H and Blott B H 1992 *J. Nucl. Mater.* **196–8** 1053–8
[5] Woods M E, Hopkins B J and McCracken G M 1985 *Surf. Sci.* **162** 929–33
[6] Wintucky E G, Curen A N and Sovey J S 1981 *Thin Solid Films* **84** 161–9
[7] Sogard M R 1980 *J. Appl. Phys.* **51** 4417–25
[8] Bruining H 1954 *Physics and Application of Secondary Electron Emission* (London: Pergamon)
[9] Everhart T E 1960 *J. Appl. Phys.* **31** 1483–90
[10] Verma R L 1977 *J. Phys. D: Appl. Phys.* **10** 1167–73
[11] Myklebust R L, Neubury D E and Yakowitz H 1976 *Use of Monte Carlo Calculations in Electron Probe Microanalysis and Scanning Electron Microscopy NBS Special Publication 460* ed K F J Hendrich, D E Neubury and H Yakowitz (Washington, DC: Dept. of Commerce)
[12] Joy D C 1991 An introduction to Monte Carlo simulations *Scan. Microsc.* **5** 329–37
[13] Liljequist D 1989 *J. Appl. Phys.* **65** 2431–8
[14] Ashley J C 1988 *J. Electron Spectrosc. Rel. Phenomena* **46** 199–214
[15] Ohya K, Nishimura J, Kawata J and Mori I *J. Nucl. Mater.* in press
[16] Valkealahti S, Schou J and Nieminen R M 1989 *J. Appl. Phys.* **65** 2258–66
[17] Joy D C and Luo S 1989 *Scanning* **11** 176–80
[18] Tung C J, Ashley J C and Ritchie R H 1979 *Surf. Sci.* **81** 427–39
[19] Neubury D E and Myklebust R L 1981 *Analytical Electron Microscopy* ed R H Geiss pp 91–8
[20] Arakawa E T, Dolfini S M, Ashley J C and Williams M W 1985 *Phys. Rev.* B **31** 8097–101
[21] Ohya K, Nishimura K and Mori I 1991 *Japan. J. Appl. Phys.* **30** 1093–4
[22] Voreades D 1976 *Surf. Sci.* **60** 325–48
[23] Willis R F, Fitton B and Painter G S 1974 *Phys. Rev.* B **9** 1926–33